were also recorded during all procedures (Grass Astro-Med Inc., Warwick RI, USA). Temperature was recorded and maintained around 36.7 ± 0.25 °C with a heater pad thermocouple (BVT-100A BRC, Tokyo, Japan) or an air-circulation heating system (3M™ Bair Hugger warming unit 750, Arizant Healthcare, St. Paul, MN, USA). The variables did not change significantly during the procedures. For infection prophylaxis, antibiotics were applied intramuscularly before starting the surgery (cefovecin sodium, Convenia 8 mg/kg, Pfizer Japan Inc., Tokyo, Japan).

AChAO. The marmoset head was fixed in a stereotaxic frame (Narishige SR-6C; Japan), and under aseptic conditions the scalp was cut between the ears and retracted anteriorly and posteriorly. The left temporal muscle was then detached from the bone and retracted. A large cranial flap from the orbital rim to the occipital bone was opened and the dura was incised. The stereotaxic frame was tilted ~30° laterally and the anterior lobe was lifted up gradually by placing small cotton balls into the space underneath. Dissection was performed in the convergence of the anterior and temporal lobe, finding the MCA origin and following the ICA until the AChA was found over the optic tract. The vessel was electrocoagulated and transected completely (20 W) using bipolar forceps (Surgitron F.F.P.F. EMC; Ellman, NY, USA). Coagulation was performed by episodes of approximately 1 s in length until the vessel was completely sectioned. Between coagulations, saline solution irrigation was used to cool down the tissues surrounding the vessel. For chronic experiments, artificial dura (Gore-Tex DM-03020, Tokyo, Japan) was used to cover the brain surface and sutured without inducing pressure; then, the temporal muscle was placed over the artificial dura and the skin was sutured (n = 5). For acute experiments, 12 marmosets were euthanized immediately after surgery and received transcardial perfusion with heparinized saline solution followed by 4% (w/v) cold paraformaldehyde and latex perfusion (as described above) to study the vascular structures (non-operated side) and to confirm the accuracy of AChA identification and occlusion (operated side). To avoid brain deformation during perfusion, the bone flap was returned over the brain and fixed using a suture between the temporal muscles before euthanasia.

Sham operations. In three animals, the protocol developed for AChAO was used, but without electro-coagulating the AChA.

Postoperative management. After surgery, a bolus injection of sugammadex (Bridion IV, 0.16 g/kg, MSD Co., Ltd., Tokyo, Japan) was administered to reverse the muscle relaxant effect. After marmosets started to breathe spontaneously, artificial ventilation and isoflurane were ceased, extubation was performed, and animals were allowed to recover in an incubator (29 °C, O2: 20% (v/v)). All animals were nursed and hand-fed after the procedure until they were able to care for themselves.

Behavioral assessment

Hand preference. Before starting the chronic experiments, marmosets were evaluated to determine their hand preference as follows: a transport cage was attached to the marmoset home cage with a modified cover consisting of a transparent acrylic panel with a rectangular window. Perpendicular to the acrylic, six PVC tubes were placed horizontally and attached to each other (inner diameter 2 cm, length 5 cm) with one opening over the window. To test the marmosets, a black panel was used to cover the marmoset side; meanwhile a sweet treat was loaded in one of the tubes. When the black panel was removed, the preferred hand to retrieve the treat was recorded. The procedure was repeated 30 times (five times per tube) on three different days using a random pattern. All marmosets used in the chronic phase of the experiments preferred the right hand. Although the same evaluation was attempted after surgery, some animals were reluctant to perform the task; for this reason, after surgery hand preference was evaluated only during volitional attempts that each marmoset made during feeding.

Freret neurologic score (FS). Before surgery and 1, 4, 7 and 10 days after surgery, the neurologic status of each animal was assessed using a neurologic score previously described by Freret et al. (2008) (FS). This test consisted in the evaluation of the absence (score = 2), scarce occurrence (score = 1) or presence (score = 0) of the following abnormal movements and postures: forelimbs/hindlimbs slipping or dangling under the perch at rest or movement, hand crossing the chest, head tilting and reaction to a visual stimulus. The highest scores were 24 points for "total score" and 10 points for "hemilateral score" (left or right evaluation of forelimb/hindlimb slipping or dangling under the perch at rest or movement and ipsilateral hand crossing the chest).

Marmoset neurologic score (MNS). Because the FS provides a gross impression of marmoset status, we considered that an additional, more detailed evaluation of natural behavior was necessary to provide a comparison point of neurologic condition in each animal. For this reason, we designed a new test (MNS) aimed to determine the presence (score = 0) or absence (score = 1) of several aspects before and at days 1, 4, 7 and 10 after surgery (Table 1). The marmoset was evaluated in the home cage before breakfast; after removing all the cage contents, an acrylic door was placed instead of the regular cage door and a camera was located in front of the cage. The initial 10 min involved video recording the spontaneous natural behavior of the marmoset. Following this, a perch and a loft were introduced into the cage, and little treats were distributed over the cage to encourage the marmoset to move around. An additional 5 min were recorded with these conditions. Finally, the marmoset was retrieved from the cage and allowed to stand in the experimenter's arm. General evaluation, "stick test" and "limb stimuli

Table 1. Marmoset neurologic score (MNS)

General evaluation	During holding in the examiner's arm	Hemilateral evaluation
Stays in back of the cage	Inadequate grasping to the examiner's arm[4]	Body tilting
Stays still for 1 min	Poor body balance[5]	Head tilting
Cannot stand in the perch	Inaccurate food targeting	Hand waving
Dysmetria[1]		Repeated touching before grasp cage bars
Required assisted feeding[2]		Hand crossing the chest
Circling behavior		Hand slipping from the cage bars
Left palpebral ptosis		Hand dangling from the cage bars
No jumping from cage walls[3]		No grasping a stick when presented
No rearing without hand support		Cannot hold a stick more than 3 s
		Absent retrieve reflex to hand stimuli[6]
		Hand neglect during feeding
		Foot slipping from the cage bars
		Foot dangling from the cage bars
		Absent retrieve reflex to foot stimuli[6]

Total score: 40 points (general, 9 points; holding, 3 points; hemilateral, 14 points per side).

[1] Dysmetria was evaluated during feeding. Marmosets trying to eat alone that could not coordinate hand–mouth movement, or attempted to aim a piece of food to the mouth but missed, were considered dysmetric.

[2] When marmosets could not finish a quarter of their food in 1 h, manual feeding was performed.

[3] Before surgery, marmosets usually jumped from one wall of the cage to another; when this behavior was absent during observation after surgery, a point was taken off.

[4] Lack of force to hold evidenced by easy slipping from the examiners arm, or resistance was minimal when the animal was grabbed by the tail and gently pulled away, in comparison to presurgical status.

[5] During holding, when the marmoset was located over the examiner's arm and the arm was moved away from the examiner's chest, if the marmoset moved from right to left while approaching the examiner's chest, a point was taken off.

[6] "Retrieve reflex" refers to the fast retrieval of the marmoset extremity when the examiner holds the animal and without intruding in the marmosets' visual field touch an extremity using a brush.

tests" (see Table 1) were performed by the experimenter. A score was calculated from the features observed in the video and a record made by the experimenter during the marmoset holding. The highest score was 40 for "total" (all points) and 14 for "hemilateral" (points for only one side of the body) evaluation.

Magnetic resonance imaging (MRI)

Prior to and 4 days after surgery, MRI images of the brain were obtained from eight marmosets. Each animal was anesthetized using pentobarbital sodium (Somnopentyl, 25 mg/kg IM., Kokuritsu Seiyaku Corp., Tokyo, Japan), and SaO2 was monitored. Temperature was maintained with a warm gel pad throughout the scanning procedure. Heads were fixed in an MRI-compatible stereotaxic frame and scanned using a 4-channel array coil on a 3 Tesla MRI (Siemens Trio, Erlangen, Germany). A three-plane localizer image was obtained to ensure correct positioning of the target images (repetition time (TR) = 100 ms, echo time (TE) = 5 ms, flip angle (FA) = 40°, field of view (FOV) = 120 mm, slice thickness = 3 mm). A three-dimensional T1-weighted image was then taken using a magnetization prepared rapid gradient echo sequence (TR = 2300 ms, TE = 2.8 ms, inversion time (TI) = 1000 ms, FA = 12°, FOV = 67 mm, image matrix = 192, in-plane voxel size = ~0.3 mm). T2-weighted images (TR = 4000 ms, TE = 520 ms, FOV = 43 mm, image matrix 128, in-plane voxel size = ~0.3 mm) were also taken.

Histology

Eleven days after surgery, marmosets were deeply anesthetized with pentobarbital sodium (Somnopentyl, 35 mg/kg IV, Kokuritsu Seiyaku Corp., Tokyo, Japan) and transcardially perfused with 300 cc of heparinized saline solution followed by 300 cc of cold 4% (w/v) paraformaldehyde in 0.1 M phosphate buffer (PB). Brains were dissected, post-fixed overnight and then immersed in 30% (w/v) sucrose in PB. Forty-micrometer-thick slices were cut across the infarcted zones confirmed by the MRI images using a freezing stage sledge microtome (REM-710, Yamato Kohki Industrial. Saitama, Japan). To assess the infarcted area, Nissl staining was performed on one in every four sections. Sections were incubated with 0.1 M PB containing 0.5% (v/v) TritonX-100 for 30 min at room temperature, washed with 0.05 M PB, mounted on precoated glass slides and dried at room temperature overnight. Samples were dehydrated by ethanol immersion, and de-fatting was performed overnight (chloroform:methyl-alcohol = 1:1). Samples were rehydrated, washed with distilled water (DW) and transferred to thionin 0.15% (w/v) solution for 30–60 s. Samples were washed again, and thionin excess was removed using ethanol. Finally, samples were cleared using xylene, and cover-slipped using Entellan-neu (Merck).

To assess WM, myelin staining (Larsen et al., 2003) was performed with some modifications. One in every four sections were incubated with 0.01 M PB containing 0.005% (v/v) Triton X-100 for 30 min at room temperature, washed with 0.05 M PB, mounted on precoated glass slides and dried at room temperature for 24 h. Samples were fixed with 4% (w/v) paraformaldehyde for 5 min, and then washed and blocked in 10% (w/v) citrate buffer twice for 2 min each. Sections were transferred to autometallographic (AMG) developer solution composed of gum Arabic (0.5 kg/ml) 270 ml, citrate buffer 45 ml, hydroquinone (0.006 g/ml) 67.5 ml and silver nitrate (0.007 g/ml) 67.5 ml (Larsen et al., 2003) in a dark chamber for 115 min, followed by the developer fixative

(fresh AMG developer solution mixed with sodium thiosulfate anhydrous 5% (w/v)) for 10 min. All reagents used were purchased from Nacalai Tesque Inc., Kyoto, Japan. After washing with DW, samples were dehydrated in ethanol, cleared with xylene and cover-slipped with DPX (Merck Millipore, Darmstadt, Germany). Pictures were taken using bright field microscopy (Keyence BZ 8000).

Image analysis

Lesion volume calculation. Injured areas were evaluated from stained slices using UTHSCSA Image Tool for windows software version 3.0 (University of Texas Health Science Center, San Antonio, TX, USA). Nissl-stained samples were used to measure the total infarcted area of each slice (infarct volume) and Myelin slices to measure the infarct areas compromising only the IC (IC infarct volume). The infarct volume and IC infarct volume were derived from the sum of the areas and slice thickness. Additionally, the left IC ratio was calculated using the myelin-stained slices (stereotactic reference: interaural +5.6 mm to +11.3 mm. Hardman and Ashwell, 2012) by measuring the left and right IC area, and calculating the volumes from sum of the left and right IC areas and slice thickness; data were expressed as a percentage by comparison of the left (infarcted) IC with the contralateral (nonimpaired) IC as described before (Puentes et al., 2012).

Infarct topographical analysis. A frequency map was constructed by hand drawing each infarct area (from Nissl staining) over myelin-stained templates (one sample set from a sham-operated animal). The original color was modified to improve the contrast with the infarcted areas (Adobe Illustrator CS 5.1., Adobe Systems Inc. CA, USA). Each marmoset infarct map was given a different color. White areas indicate overlapping of three different colors. Thinned color areas indicate the overlapping of two different colors.

Statistical analysis

Statistical analyses were performed using R software (version 3.1.0). Error bars are expressed as the standard deviation of the data. Dixon test type 10 was used to determine the outliers; later, the relation between the parameters was calculated by using a linear mixed model (Latin square test). Subsequently, an analysis of variance (ANOVA) was applied followed by the pairwise *t*-test with Bonferroni correction for group analysis. Finally, a Tukey honestly significant difference (HSD) simultaneous test was conducted to evaluate significant differences among groups in a time-dependent manner.

RESULTS

Marmoset vascular distribution resembles the human anatomy

In all marmosets, the vascular pattern resembled the human anatomy finding a complete Willis circle (Fig. 1A).

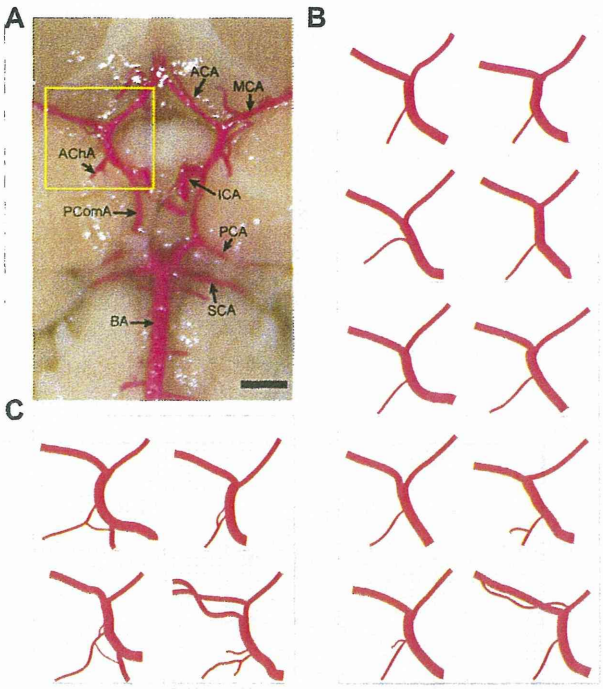

Fig. 1. Anterior choroidal artery (AChA) of the common Marmoset. (A) Cadaveric preparation showing the AChA bilaterally emerging from the internal carotid artery (ICA). Both temporal lobes were removed. The yellow square marks the area drawn in B and C (right side). (B) Animals (n = 10) with a unique AChA emerging from the lateral aspect of the ICA before its bifurcation resembled the human vasculature. (C) Unusual patterns of the AChA were observed in some animals (n = 4), which were characterized by a bifurcated origin and/or an additional branch from the posterior communicating artery (PcomA). BA, basilar artery; PCA, posterior cerebral artery; SCA, superior cerebellar artery. Scale bar = 2 mm. (For interpretation of the references to color in this figure legend, the reader is referred to the web version of this article.)

In 10 animals, the AChA sprouted from the ICA between the posterior communicating artery (PcomA) and the ICA bifurcation (Fig. 1B), running over the optic tract (AChA-ICA bifurcation: 1.4 mm ± 0.2 mm). Four animals exhibited some anatomical variations (Fig. 1C) where duplicated or triplicated AChA origins converged in a single main artery or an aberrant AChA was found. In two cases (Fig. 1C, left column), one of the additional origins emerged from the PcomA instead of the ICA. The distance from the main branch of the AChA to the bifurcation of the ICA was 1.6 mm (±0.18). In humans, it is well known that the AChA is a main feeder artery of the IC (Hupperts et al., 1994; Ois et al., 2009). Therefore, if the anatomical distribution of this artery is close between humans and marmosets, its occlusion might lead to infarction of the IC.

Development of the surgical protocol

A large craniotomy was required to expose the deep structures of the brain (Fig. 2), and the left AChA was found behind the temporal lobe being the last branch before the ICA bifurcation (Figs. 2B, 3A, B). When two arteries were found emerging at the expected place of

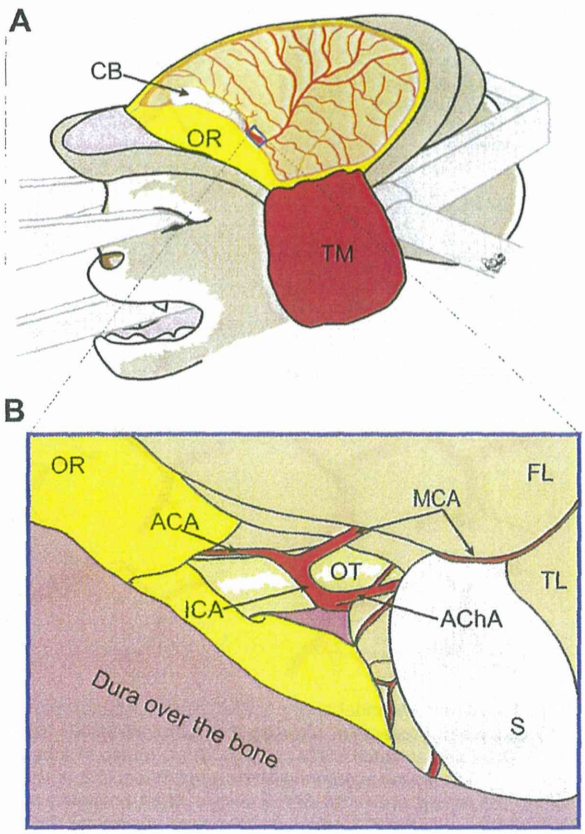

Fig. 2. Surgical approach to the anterior choroidal artery (AChA). After head fixation, skin coronal incision, detachment and retraction of the temporal muscle (TM) a hemicraniotomy was performed. (A) Cotton balls (CB) were used to lift up the frontal lobe (FL). (B) Magnification of the blue square in C. A spatula (S) was used to retract the temporal lobe (TL) to find the AChA over the optic tract (OT). The bifurcation of the internal carotid artery (ICA) into the middle cerebral (MCA) and anterior cerebral arteries (ACA) can be seen. FL, frontal lobe; ICA, internal carotid artery; OR, orbital rim. (For interpretation of the references to color in this figure legend, the reader is referred to the web version of this article.)

the AChA, both were coagulated and sectioned. Latex injection performed after AChAO confirmed the complete section of the AChA (Fig. 3C) in 92% (11/12) of the marmosets. One marmoset had an additional branch bypassing the AChA to the PcomA, so the occlusion of the branch visible during the surgery was insufficient to cut the bloodstream to the AChA.

AChAO induced motor behavioral changes

Before surgery, all animals (n = 8) showed top scores for both FS (total = 25 points, hemilateral = 10 points per each side) and MNS (total = 40 points, hemilateral = 14 points per each side). After AChAO (n = 5), we noticed heterogeneous behavior of the operated animals. After individual evaluation, three marmosets manifested right sided neurologic deficits, as measured by the applied scores (FS and MNS), and required longer nursing and hand feeding during the observation period. Conversely, the remaining two marmosets recovered faster after surgery, and by day 11 their behavior was comparable to the status before surgery when the scores were applied. To group the animals that underwent AChAO with respect to their behavior, a Dixon test type 10 for outliers was applied to the total MNS score, finding the animals with higher scores as outliers ($P < 0.01$ for days 7 and 10). Operated animals were then divided into two groups: AChAO with neurologic deficits (AChAO + ND: n = 3) and AChAO without neurologic deficits (AChAO – ND: n = 2). For FS and MNS, the AChAO + ND group showed a reduction in total and right side scores in comparison with AChAO – ND and sham-operated animals, which was more pronounced for MNS (Fig. 4; AChAO + ND, Tukey HSD simultaneous tests: $^{*}P < 0.05$, $^{**}P < 0.01$). These animals also required longer periods to eat by themselves, requiring hand feeding until day 5–7. Additionally, they shifted the hand preference to the left side when attempting to eat by themselves. The AChAO – ND group showed a slight reduction in scores, which quickly improved over time (Fig. 4, AChAO – ND). This group also required less nursing and 2–3 days after surgery started to eat by themselves. One marmoset kept using his right hand as the preferred one, and the other marmoset increased use of his left hand without neglecting the right one during feeding. Left side scores did not change after surgery for any group. Sham-operated animals recovered fast after surgery and nursing requirement was minimal. Hand preference did not change after surgery. There was no statistical difference between AChAO – ND and sham groups (Tukey HSD simultaneous tests: $P > 0.05$).

AChAO induced damage to the IC

MRI performed 4 days after surgery showed injury extending from the genu to the posterior limb of the IC in the AChAO + ND group (Fig. 5A); extension of the infarction to surrounding structures differed between animals, but the posterolateral expansion was common in the three marmosets (Fig. 5A, D). The findings of AChAO – ND group were different: one animal did not show IC compromise, and the other showed a small infarction located medially in the genu of the IC without posterolateral expansion as observed in the AChAO + ND group (Fig. 5B, E). Animals from the sham group did not show relevant changes.

Histology showed IC impairment congruent with MRI findings. For the AChAO + ND group, myelin staining showed important demyelination of the IC at the infarct level and Nissl staining showed dense infiltrates affecting the IC and expanding briefly to surrounding structures (Fig. 6A). The AChAO – ND group showed small demyelinated zones accompanied by cell infiltration in the optic tract and basal ganglia, and one marmoset showed a small demyelinated zone in the genu of the IC (Fig. 6B). Sham-operated animals did not show relevant changes. The left IC ratio was briefly reduced for the AChAO + ND (85.67% ± 5.62) and AChAO – ND (94.76%) groups because WM was lost at the IC for the AChAO-operated animals in comparison to the sham group (99.74% ± 0.66). However, the infarct volume

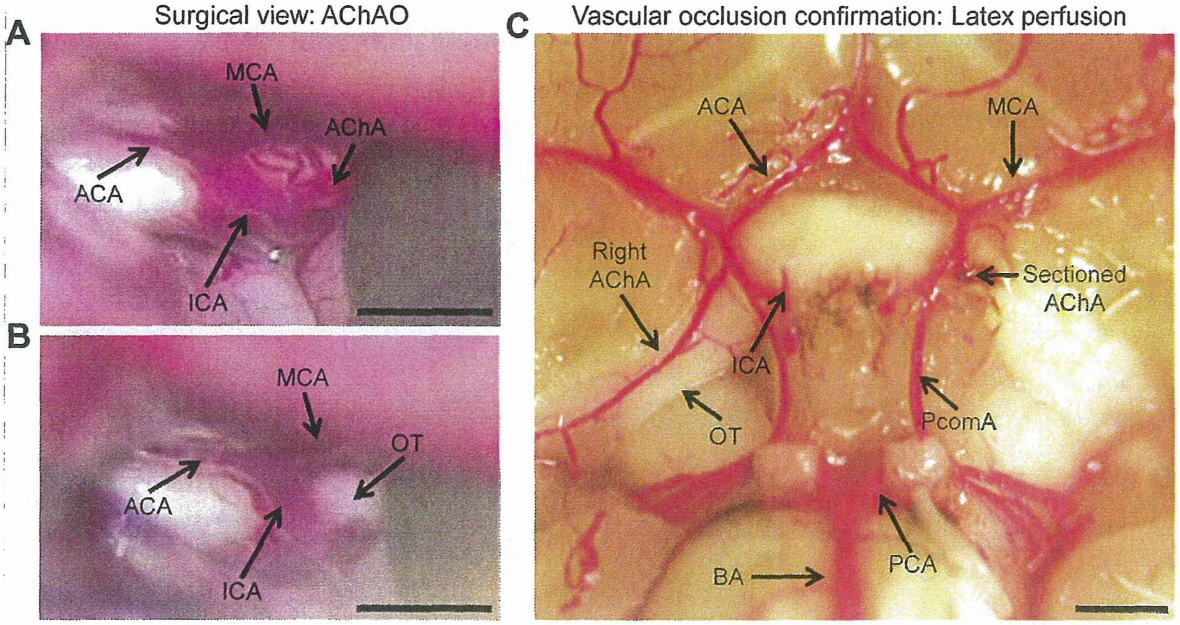

Fig. 3. Anterior choroidal artery occlusion. (A) Visualization of the anterior choroidal artery (AChA) emerging from the ICA during the surgical procedure. (B) Same location as A, after AChA occlusion; there was no damage to the ICA or to the optic tract (OT). (C) Vascular occlusion confirmation: latex injection was performed immediately after surgery to evaluate the accuracy of the vessel identification and its complete electrocoagulation. ACA, anterior cerebral artery; BA, basilar artery; MCA, middle cerebral artery; PCA, posterior cerebral artery; PcomA, posterior communicating artery. Bars = 2 mm.

was markedly larger for the AChAO + ND than AChAO – ND group (AChAO + ND: 18.41 mm^3 ± 9.75 AChAO – ND: 2.97 mm^3) as the IC infarct volume (AChAO + ND: 3.06 mm^3 ± 0.40. AChAO – ND: 0.14 mm^3). Infarct frequency maps revealed concomitant damage to the IC in AChAO + ND group (Fig. 6C) in contrast to the smaller infarct in AChAO – ND group (Fig. 6D).

DISCUSSION

In this study, we found that the marmoset vascular distribution was generally similar to the pattern found in the human brain (Fig. 1) with a complete circle of Willis and an AChA running over the optic tract (Wiesmann et al., 2001; Uz et al., 2005). However, there was evidence of anatomical variations (Fig. 1C), which were expected given their presence in humans. An intraoperative anatomical study performed in humans by Akar et al. (2009) found that 86.4% of the evaluated patients had a single AChA emerging from the ICA; the remaining patients showed different branching patterns and in some cases duplicated or triplicated AChAs were found. This anatomical variability broadens the spectrum of clinical conditions for AChA stroke patients. In our study, marmosets that underwent AChAO showed different behavior during the observation period. It is likely that a nonvisible AChA branch during the surgical procedure bypassed the blood flow to the distal AChA reducing the impact of the artery occlusion in two of the operated animals that did not show neurologic impairment (Fig. 6D, AChAO – ND). Although this feature reduces the reproducibility of the model, conditions are similar to the human reproducing also the anatomical variations at some level. Additionally, the medial lenticulostriate arteries from the MCA and some perforating branches from the ICA can provide blood flow to the posterior limb of the IC (Ghika et al., 1990). This condition may influence infarct size. Visualization of the IC irrigation state before surgery may provide relevant information for future research.

MRI images and histological preparations (chronic experiments) showed that the AChAO was able to induce a small infarction affecting the IC, and other subcortical structures in animals with evident neurologic deficits (Figs. 5 and 6; AChAO + ND). Despite the smaller size in infarct in comparison with previous MCAO studies performed in marmosets (Marshall and Ridley, 2003; Freret et al., 2008), the neurological deficit was still evident 10 days after surgery (Fig. 4). Overall, these results clearly suggest that the AChAO is a feasible technique able to induce an infarction affecting the marmoset IC with consequent motor deficits, and is the first described WM stroke model in the marmoset monkey.

Other studies implementing the AChAO

As far as we know, the AChAO model has only been proposed in one previous study made by Tanaka et al. (2008) in miniature pigs; they reported a high rate of success for brain infarct induction (91.4%) when an aneurism clip was placed or electrocoagulation was performed in the proximal AChA. As an advantage, their study was generated in an animal species with a gyrencephalic brain and the AChAO was able to induce motor impairment. However, recovery occurred within 10 days even though a clear IC injury was observed 4 weeks after surgery.

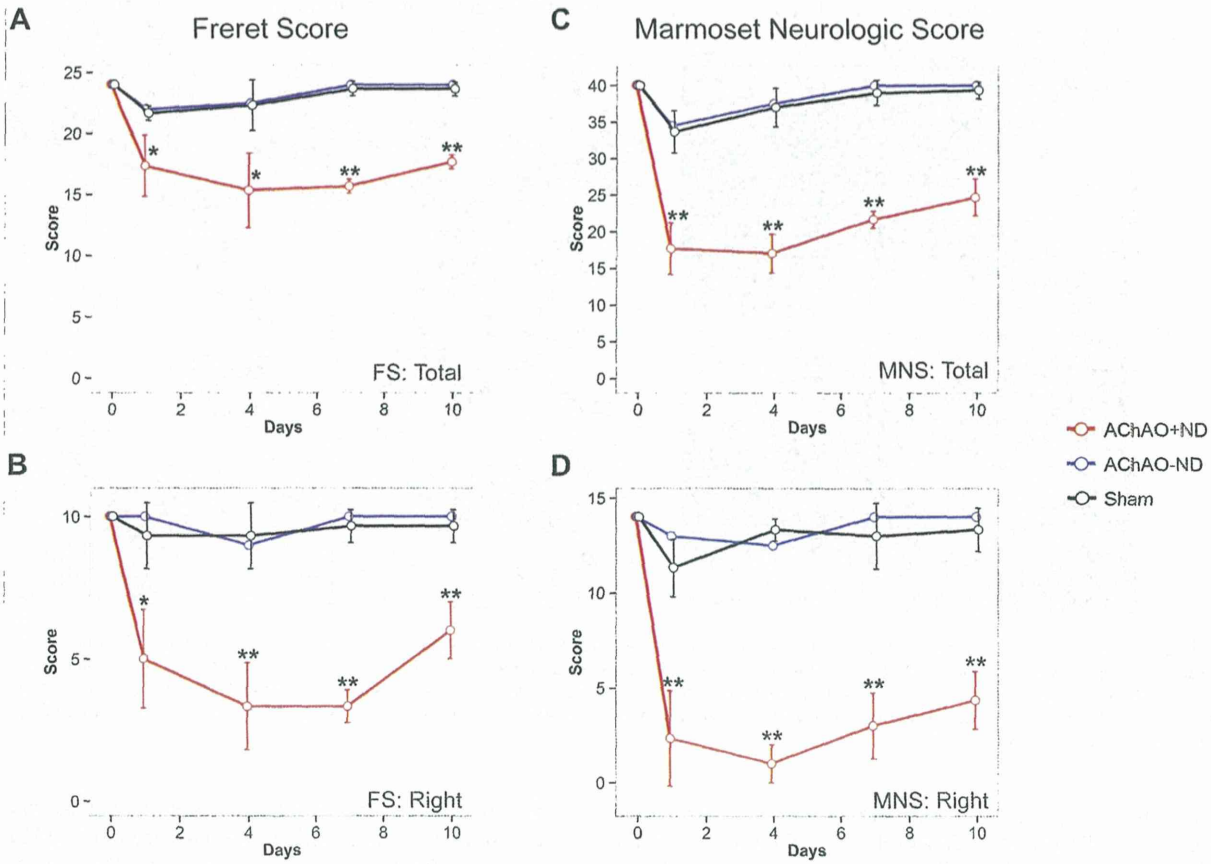

Fig. 4. Behavioral changes after surgery. Existing (Freret Score: FS) and newly developed behavioral tests (Marmoset Neurologic Score: MNS) were used to assess behavioral changes after surgery in all animals. Animals that underwent AChAO were divided in two groups regarding their behavior: AChAO animals showing neurologic deficits (AChAO + ND) and AChAO animals without neurologic deficits (AChAO – ND); see text for details. For FS, total (A) and right-hemilateral (B) scores decreased in the AChAO + ND group when compared with the AChAO – ND and sham groups (*$P < 0.05$, **$P < 0.01$). The MNS was also applied showing similar results for total (C) and right-hemilateral (D) scores (**$P < 0.01$). Significance among groups was established using a linear mixed model followed by ANOVA and Tukey HSD simultaneous test.

By contrast, our marmosets exhibited motor impairment even at day 10 (Fig. 4, AChAO + ND). This discrepancy could be ascribed to the vascular anatomical differences between species that may affect the functional recovery of the animals. In the miniature pig, triplicated MCAs emerge from the ICA (Imai et al., 2006), suggesting the existence of a higher number of lenticulostriatal arteries. This condition may improve collateral blood flow to the IC after AChAO, thus attenuating the ischemic impact and allowing fast neurological recovery. By contrast, the brain vasculature of the marmoset resembles the human's (Fig. 1A), with a single MCA and an AChA with a similar anatomical pattern in most cases. Because blood flow supported by the lenticulostriatal arteries is likely to be similar in species with a unique MCA, we can infer that the motor deficit evidenced in the AChAO may not be reversible as seen in AChA stroke patients.

Animal species selection for stroke research

Stroke research has been conducted mainly in rodents owing to their handling and reproduction rate advantages (Macrae, 2011; Canazza et al., 2014). However, owing to translational research failure from several therapeutic approaches tested in these species (Xu and Pan, 2013), the development of novel stroke models in different animal species is required. Owing to their phylogenetic similarities to humans, the NHP has drawn attention for the generation of new stroke models (Fukuda and del Zoppo, 2003). However, the use of gyrencephalic NHPs, such as the baboon or macaque, is restricted owing to their size, care and breeding requirements. Nevertheless, the common marmoset is a NHP species relatively easy to house and handle owing to their small size (~300 g) and high reproduction ratio (Abbott et al., 2003; Okano et al., 2012). Therefore, marmosets offer a rich scenario for stroke research balancing resemblance to human features, closer ergonomics and smaller GM/WM ratio in an animal that is easier to handle than a larger NHP.

Clinical relevance

AChA territory infarctions account for 2.9–11% of all patients with acute ischemic stroke (Hamoir et al., 2004; Ois et al., 2009) and are frequently associated with motor deficits (Palomeras et al., 2008), where IC involvement correlates importantly with motor outcome (Nelles et al., 2008). Induced hemiparesis can be severe and progressive (Steinke and Ley, 2002). Owing to the catastrophic

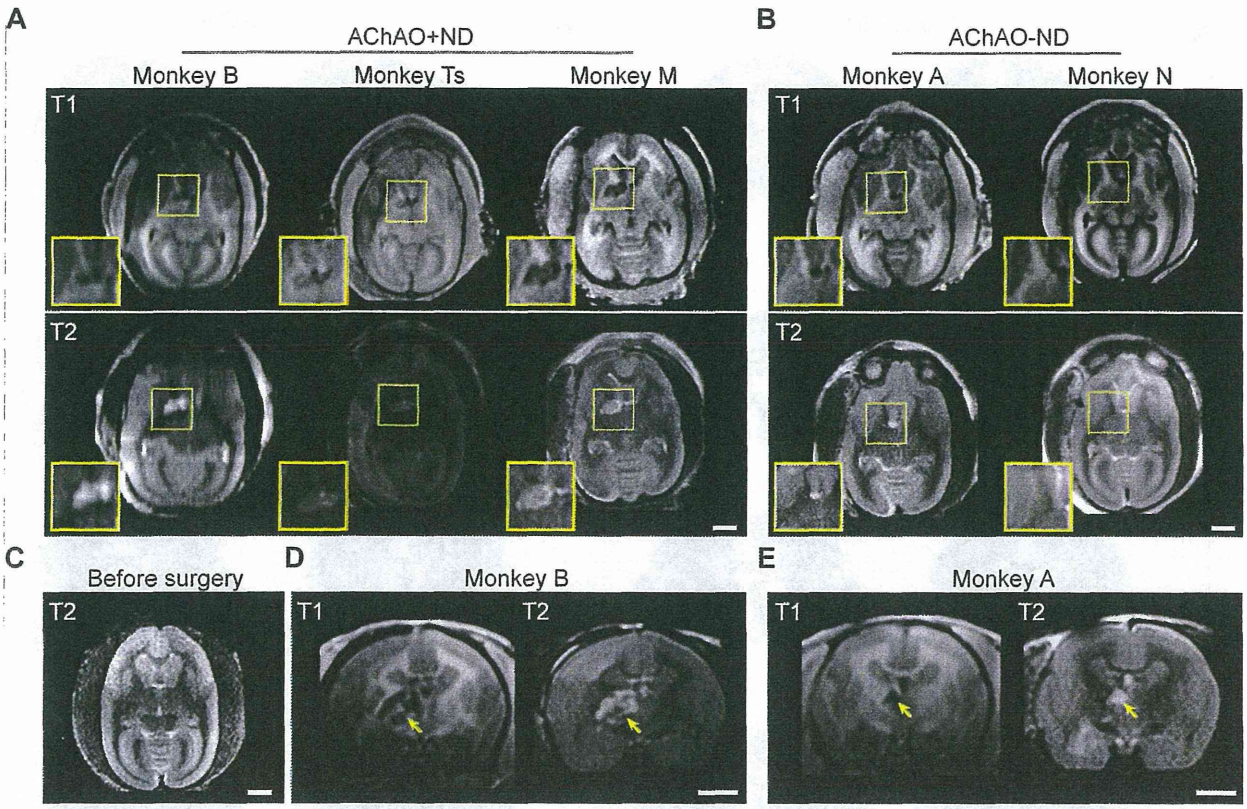

Fig. 5. Infarct extension at day 4. T1 and T2 weighted images (WI, axial projections) from each monkey after AChAO. (A) Monkeys showing neurologic deficits (AChAO + ND). (B) Monkeys without neurologic deficits (AChAO – ND). Yellow squares enclosing the infarct are zoomed on the left side of each image. (C) T2WI (axial projection) from one animal before surgery. (D) T1WI and T2WI (coronal projections) from one animal belonging to the AChAO + ND group. (E) T1WI and T2WI (coronal projections) from one animal belonging to the AChAO – ND group. Yellow arrows indicate infarction. Scale bar = 5 mm. (For interpretation of the references to color in this figure legend, the reader is referred to the web version of this article.)

conditions of AChA stroke patients, where human studies directly correlate WM damage to motor outcome after stroke (Puig et al., 2011), we consider studies focusing on damage to the IC will provide more relevant information and aid in the search for new strategies to improve recovery from motor function deficits.

Limitations of the model

This model was developed in a common marmoset aiming to generate a NHP model that could be easily comparable to the human condition. Although phylogenetically humans and marmosets are closer than rodents or other inferior mammals, the marmoset brain is still lissencephalic. Despite the increased WM ratio in comparison with rodents, the cortical distribution is quite different to the human. It is important to remember such differences across species for translational research.

A second limitation refers to the possibility to design a reperfusion model by occluding the AChA that may allow the evaluation of pharmacological interventions targeting the reperfusion phase following ischemia (Macrae, 2011). Our initial design was to occlude the AChA using an aneurism clip. However, owing to space restrictions it was not possible to use this approach. Instead we decided to perform a permanent occlusion of the vessel. These conditions did not allow us to evaluate the reperfusion state after stroke. Further surgical procedures need to be developed to overcome this difficulty.

Third, we found neurologic impairment only in 60% of operated marmosets, which is a low rate of success in comparison with the established stroke models for rodents (Tamura et al., 1981; Kohno et al., 1995) and marmosets (Marshall and Ridley, 2003; Freret et al., 2008). This lower success rate could be a disadvantage for applying this model for translational research in the development of neuroprotective drugs as well as cell therapies due to the requirement of a large number of animals.

Fourth, our model may not be directly applicable to the majority of human stroke studies because AChA stroke in humans is relatively rare in comparison with major infarctions such as MCA stroke (Rordorf et al., 1998). However, by establishing the AChA stroke model, we wanted to offer an opportunity to study the WM ischemia process without impairing the cortex. Therefore, we believe this model may be comparable to any human stroke that is accompanied by WM ischemia.

Future directions

The AChAO method in marmoset monkeys established in this study will allow us to perform a detailed examination of motor dysfunction and recovery using previously reported behavioral evaluations (Marshall and Ridley,

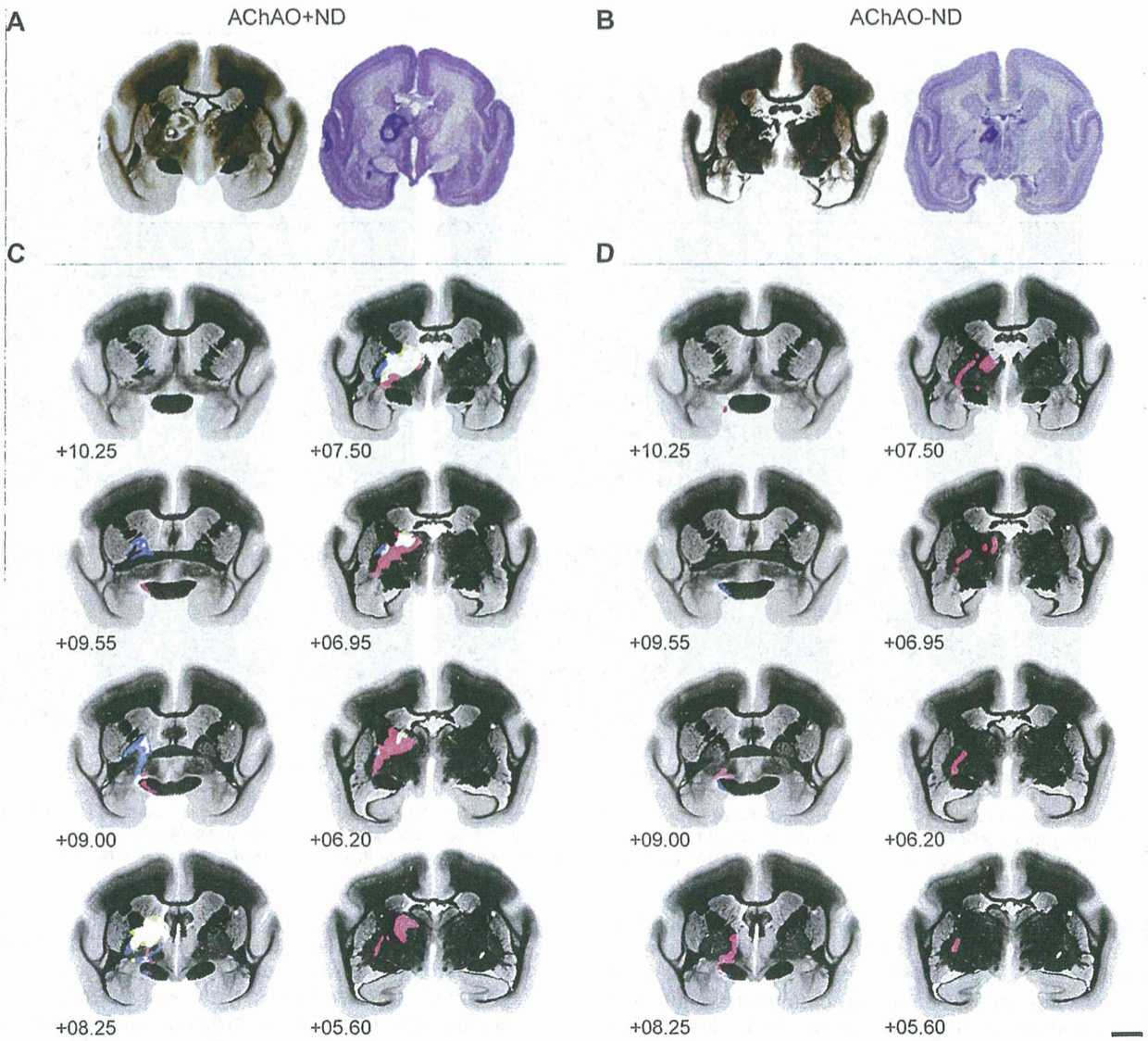

Fig. 6. Topographical distribution of infarction. Histological preparations (day 11) for Myelin (left) and Nissl staining (right) from one animal who showed behavioral deficits after surgery (A, AChAO + ND) and one who did not (B, AChAO – ND). Frequency maps were constructed by drawing the infarct areas to the corresponding level for AChAO + ND (C) and AChAO – ND groups (D). Semi-transparencies represent two samples overlapped; white color represents confluence of three samples (C only). Brain templates were constructed from myelin staining of a control animal. Numbers indicate the stereotaxic reference from the interaural line (Hardman and Ashwell, 2012). Scale bar = 3 mm. (For interpretation of the references to color in this figure legend, the reader is referred to the web version of this article.)

2003; Freret et al., 2008) and additional evaluations such as gait pattern, pressure distribution and muscular synergy alterations after WM stroke. Additionally, showing the physiological mechanism for damaged IC compensation by other descending or cortical and subcortical networks will have a crucial implication on the establishment of novel rehabilitation strategies in human stroke patients.

CONCLUSIONS

The occlusion of the AChA in marmosets was able to induce a focal infarction that compromised the IC, and resulted in neurologic deficits, which were evident during natural behavior and that were sustained to day 10. This model offers a new approach to understand the pathological process of WM ischemia, as well as stroke treatment, including pharmacological therapies and physiotherapy routines, allowing the development of new strategies that focus on improving motor function after WM impairment.

FUNDING

This work was supported by an Intramural Research Grant for Neurological and Psychiatric Disorders from the National Center of Neurology and Psychiatry, innovative areas "Understanding brain plasticity on body representations to promote their adaptive functions (Grant No. 26120003)" from the Ministry of Education,

Culture, Sports, Science and Technology of Japan, and the Japan Science and Technology Agency Precursory Research for Embryonic Science and Technology program to K.S.

DISCLOSURES

The authors report no conflicts of interest.

Acknowledgments—We thank Dr. Hidetoshi Ishibashi and Chika Sasaki for surgical support, Dr. Naotaka Fuji for surgical advice, Kazuhisa Sakai and Takako Suzuki for histochemical advice.

REFERENCES

Abbott DH, Barnett DK, Colman RJ, Yamamoto ME, Schultz-Darken NJ (2003) Aspects of common marmoset basic biology and life history important for biomedical research. Comp Med 53:339–350.

Akar A, Sengul G, Aydin IH (2009) The variations of the anterior choroidal artery: an intraoperative study. Turk Neurosurg 19:349–352.

Alvernia JE, Pradilla G, Mertens P, Lanzino G, Tamargo RJ (2010) Latex injection of cadaver heads: technical note. Neurosurgery 67:362–367.

Astrup J, Siesjö B, Symon L (1981) Thresholds in cerebral ischemia – the ischemic penumbra. Stroke 12:723–725.

Bailey EL, McCulloch J, Sudlow C, Wardlaw JM (2009) Potential animal models of lacunar stroke: a systematic review. Stroke 40:451–458.

Canazza A, Minati L, Boffano C, Parati E, Binks S (2014) Experimental models of brain ischemia: a review of techniques, magnetic resonance imaging, and investigational cell-based therapies. Front Neurol 19:1–15.

Derflinger S, Fiebach J, Böttger S, Haberl R, Audebert H, Heinrich J (2013) The progressive course of neurological symptoms in anterior choroidal artery infarcts. Int J Stroke. http://dx.doi.org/10.1111/j.1747-4949.2012.00953.x.

Dijkhuizen RM, Ren J, Mandeville JB, Wu O, Ozdag FM, Moskowitz MA, Rosen BR, Finklestein SP (2001) Functional magnetic resonance imaging of reorganization in rat brain after stroke. Proc Natl Acad Sci USA 98:12766–12771.

Donnan GA, Fisher M, Macleod M, Davis SM (2008) Stroke. Lancet 371:1612–1623.

Freret T, Bouet V, Toutain J, Saulnier R, Pro-Sistiaga P, Bihel E, Mackenzie ET, Roussel S, Schumann-Bard P, Touzani O (2008) Intraluminal thread model of focal stroke in the non-human primate. J Cereb Blood Flow Metab 28:786–796.

Frost S, Barbay S, Mumert M, Stowe A, Nudo R (2006) An animal model of capsular infarct: endothelin-1 injections in the rat. Behav Brain Res 169:206–211.

Fukuda S, del Zoppo GJ (2003) Models of focal cerebral ischemia in the nonhuman primate. ILAR J 44:96–104.

Ghika JA, Bogousslavsky J, Regli F (1990) Deep perforators from the carotid system. Arch Neurol 47:1097–1100.

Hamoir X, Grandin C, Peeters A, Robert A, Cosnard G, Duprez T (2004) MRI of hyperacute stroke in the AChA territory. Eur Radiol 14:417–424.

Hardman CD, Ashwell KWS (2012) Stereotaxic and chemoarchitectural atlas of the brain of the common marmoset (*Callithrix jacchus*). Boca Raton: CRC Press/Taylor and Francis Group. p. 110–198.

Hughes PM, Anthony DC, Ruddin M, Botham MS, Rankine EL, Sablone M, Baumann D, Mir AK, Perry VH (2003) Focal lesions in the rat central nervous system induced by endothelin-1. J Neuropathol Exp Neurol 62:1276–1286.

Hupperts RM, Lodder J, Heuts-van Raak EP, Kessels F (1994) Infarcts in the anterior choroidal artery territory: anatomical distribution, clinical syndromes, presumed pathogenesis and early outcome. Brain 117:825–834.

Imai H, Konno K, Nakamura M, Shimizu T, Kubota C, Seki K, Honda F, Tomizawa S, Tanaka Y, Hata H, Saito N (2006) A new model of focal cerebral ischemia in the miniature pig. J Neurosurg 104:123–132.

Koga M, Reutens DC, Wright P, Phan T, Markus R, Pedreira B, Fitt G, Lim I, Donnan GA (2005) The existence and evolution of diffusion-perfusion mismatched tissue in white and gray matter after acute stroke. Stroke 36:2132–2137.

Kohno K, Back T, Hoehn-Berlage M, Hossman KA (1995) A modified rat model of middle cerebral artery thread occlusion under electrophysiological control for magnetic resonance investigations. Magn Reson Imaging 13:65–71.

Larsen M, Bjarkam C, Stoltenberg M, Sørensen J, Danscher G (2003) An autometallographic technique for myelin staining in formaldehyde-fixed tissue. Histol Histopathol 18:1125–1130.

Lecrux C, McCabe C, Weir CJ, Gallagher L, Mullin J, Touzani O, Muir KV, Lees KR, Macrae IM (2008) Effects of magnesium treatment in a model of internal capsule lesion in spontaneously hypertensive rats. Stroke 39:448–454.

Likitjaroen Y, Suwanwela NC, Mitchell AJ, Lerdlum S, Phanthumchinda K, Teipel SJ (2012) Isolated motor neglect following infarction of the posterior limb of the right internal capsule: a case study with diffusion tensor imaging-based tractography. J Neurol 259:100–105.

Macrae IM (2011) Preclinical stroke research – advantages and disadvantages of the most common rodent models of focal ischaemia. Br J Pharmacol 164:1062–1078.

Marshall JW, Ridley RM (2003) Assessment of cognitive and motor deficits in a marmoset model of stroke. ILAR J 44:153–160.

Mergenthaler P, Meisel A (2012) Do stroke models model stroke? Dis Model Mech 5:718–725.

Muñoz Maniega S, Bastin ME, Armitage PA, Farrall AJ, Carpenter TK, Hand PJ, Cvoro V, Rivers CS, Wardlaw JM (2004) Temporal evolution of water diffusion parameters is different in grey and white matter in human ischaemic stroke. J Neurol Neurosurg Psychiatry 75:1714–1718.

Nelles M, Gieseke J, Flacke S, Lachenmayer L, Schild H, Urbach H (2008) Diffusion tensor pyramidal tractography in patients with anterior choroidal artery infarcts. AJNR Am J Neuroradiol 29:488–493.

Neumann-Haefelin T, Kastrup A, de Crespigny A, Yenari MA, Ringer T, Sun GH, Moseley ME (2000) Serial MRI after transient focal cerebral ischemia in rats: dynamics of tissue injury, blood–brain barrier damage, and edema formation. Stroke 31:1965–1972.

Ois A, Cuadrado-Godia E, Solano A, Perich-Alsina X, Roquer J (2009) Acute ischemic stroke in anterior choroidal artery territory. J Neurol Sci 281:80–84.

Okano H, Hikishima K, Iriki A, Sasaki E (2012) The common marmoset as a novel animal model system for biomedical and neuroscience research applications. Semin Fetal Neonatal Med 17:336–340.

Palomeras E, Fossas P, Cano AT, Sanz P, Floriach M (2008) Anterior choroidal artery infarction: a clinical, etiologic and prognostic study. Acta Neurol Scand 118:42–47.

Puentes S, Kurachi M, Shibasaki K, Naruse M, Yoshimoto Y, Mikuni M, Imai H, Ishizaki Y (2012) Brain microvascular endothelial cell transplantation ameliorates ischemic white matter damage. Brain Res 1469:43–53.

Puig J, Pedraza S, Blasco G, Daunis-I-Estadella J, Prados F, Remollo S, Prats-Galino A, Soria G, Boada I, Castellanos M, Serena J (2011) Acute damage to the posterior limb of the internal capsule on diffusion tensor tractography as an early imaging predictor of motor outcome after stroke. AJNR Am J Neuroradiol 32:857–863.

Rascol A, Clanet M, Manelfe C, Guiraud B, Bonafe A (1982) Pure motor hemiplegia: CT study of 30 cases. Stroke 13:11–17.

Rordorf G, Koroshetz WJ, Copen WA, Cramer SC, Schaefer PW, Budzik RF, Schwamm LH, Buonanno F, Sorensen AG, Gonzalez G (1998) Regional ischemia and ischemic injury in patients with

acute middle cerebral artery stroke as defined by early diffusion-weighted and perfusion-weighted MRI. Stroke 29:939–943.

Rosso C, Colliot O, Valabrègue R, Crozier S, Dormont D, Lehéricy S, Samson Y (2011) Tissue at risk in the deep middle cerebral artery territory is critical to stroke outcome. Neuroradiology 53:763–771.

Rosso C, Valabregue R, Attal Y, Vargas P, Gaudron M, Baronnet F, Bertasi E, Humbert F, Peskine A, Perlbarg V, Benali H, Lehéricy S, Samson Y (2013) Contribution of corticospinal tract and functional connectivity in hand motor impairment after stroke. PLoS One 8:1–11.

Sozmen EG, Hinman JD, Carmichael ST (2012) Models that matter: white matter stroke models. Neurotherapeutics 9:349–358.

Steinke W, Ley S (2002) Lacunar stroke is the major cause of progressive motor deficits. Stroke 33:1510–1516.

Tamura A, Graham DI, McCulloch J, Teasdale GM (1981) Focal cerebral ischaemia in the rat: 1. Description of technique and early neuropathological consequences following middle cerebral artery occlusion. J Cereb Blood Flow Metab 1:53–60.

Tanaka Y, Imai H, Konno K, Miyagishima T, Kubota C, Puentes S, Aoki T, Hata H, Takata K, Yoshimoto Y, Saito N (2008) Experimental model of lacunar infarction in the gyrencephalic brain of the miniature pig: neurological assessment and histological, immunohistochemical, and physiological evaluation of dynamic corticospinal tract deformation. Stroke 39:205–212.

Thomalla G, Glauche V, Koch M, Beaulieu C, Weiller C, Röther J (2004) Diffusion tensor imaging detects early Wallerian degeneration of the pyramidal tract after ischemic stroke. NeuroImage 22:1767–1774.

Uz A, Erbil KM, Esmer AF (2005) The origin and relations of the anterior choroidal artery: an anatomical study. Folia Morphol 64:269–272.

Wiesmann M, Yousry I, Seelos KC, Yousry TA (2001) Identification and anatomic description of the anterior choroidal artery by use of 3D-TOF source and 3D-CISS MR imaging. AJNR Am J Neuroradiol 22:305–310.

Xu SY, Pan SY (2013) The failure of animal models of neuroprotection in acute ischemic stroke to translate to clinical efficacy. Med Sci Monit Basic Res 19:37–45.

Zhang K, Sejnowski TJ (2000) A universal scaling law between gray matter and white matter of cerebral cortex. Proc Natl Acad Sci USA 97:5621–5626.

(Accepted 1 October 2014)
(Available online 20 October 2014)

教育総説

Review-Essentials

中脳赤核と運動機能
—系統発生的観点から—

Red Nucleus and Its Motor Function
—A Phylogenetic Perspective—

大屋知徹　関　和彦
国立精神・神経医療研究センター　モデル動物開発研究部

Key words：
rubrospinal tract
rubroolivary tract
rubral tremor

Spinal Surgery **28** (3) 258-263, 2014

日本脊髄外科学会機関誌
『脊髄外科　SPINAL SURGERY』
VOL. 28 NO. 3　2014 年 12 月

教育総説

Review-Essentials

中脳赤核と運動機能
—系統発生的観点から—

Red Nucleus and Its Motor Function
—A Phylogenetic Perspective—

大屋知徹　関　和彦
国立精神・神経医療研究センター モデル動物開発研究部

Key words：
rubrospinal tract
rubroolivary tract
rubral tremor

Spinal Surgery 28 (3) 258-263, 2014

要　旨

1）霊長類の赤核には，局在する位置，細胞構築，連絡する回路構造など，その解剖学的特徴から明瞭な区分（おもに大細胞性と小細胞性）が存在し，それぞれの機能には大きな差異がある．

2）赤核の各区分における細胞群の発達の程度は，哺乳類の中で大きなバリエーションがあり，四足歩行動物では赤核脊髄路が，高等霊長類では赤核オリーブ路が発達している．ヒトにおいてこの差異は極端であり，前者の赤核脊髄路はほぼ退化し痕跡的となっている．このため，齧歯類，ネコ，さらにはサルにおける実験結果から得られた知見を直接ヒトに外挿するには慎重を要する．

3）ヒトにおいて特異的に発達した小細胞性赤核の具体的，詳細な機能についてはほとんどわかっていないが，その臨床病態の像や破壊損傷によって作出された実験動物の機能異常から，小細胞性赤核は振戦への関わりがある．

はじめに

赤核は中脳被蓋部腹側，動眼神経核の側方に位置する赤色の核で，ヒトの脳図譜などや連続切片をみると，中脳被蓋部において大きな部分を占める核である．赤核は名前の由来となったその薄い赤色や中脳の中で占める領域の大きさから，古くからよく知られている神経核である一方，その機能については十分には理解されていない．本総説においては赤核に関する従来の系統発生的，比較解剖学的研究を俯瞰し，特に運動制御において赤核が担う機能やその障害の影響を中心に，生理学的観点から概説を試みる．

なお，赤核脊髄路については山下[1]，赤核症候群についての詳細な記述は今井[2]，振戦とのかかわりについては大江[3,4]が日本語の総説でそれぞれ詳細にまとめている．比較解剖学的視点から赤核を詳説したものは小川ら[5,6]のものがある．英語によるものは，脊椎動物の系統発生と赤核の発達については ten Donkelaar[7]，哺乳類の赤核については Massion[8]，赤核の臨床病態に関してまとめたものについては Nathan ら[9]などがある．興味のある読者は参考にされたい．

1．赤核の系統発生

赤核は中脳被蓋部の腹側，動眼神経核の横に位置する核で，脊髄への下行路，赤核脊髄路（モナコフ氏束）の起始核である．赤核が精力的に研究されたのは神経解剖学の黎明期，比較神経解剖学が盛んに行われていた時代

国立精神・神経医療研究センター モデル動物開発研究部／〒187-8502 小平市小川東町 4-1-1〔連絡先：関　和彦〕
Address reprint requests to：Kazuhiko Seki, Ph.D., Department of Neurophysiology, National Center of Neurology and Psychiatry, 4-1-1 Ogawa-higashi-cho, Kodaira-shi, Tokyo 187-8502, Japan

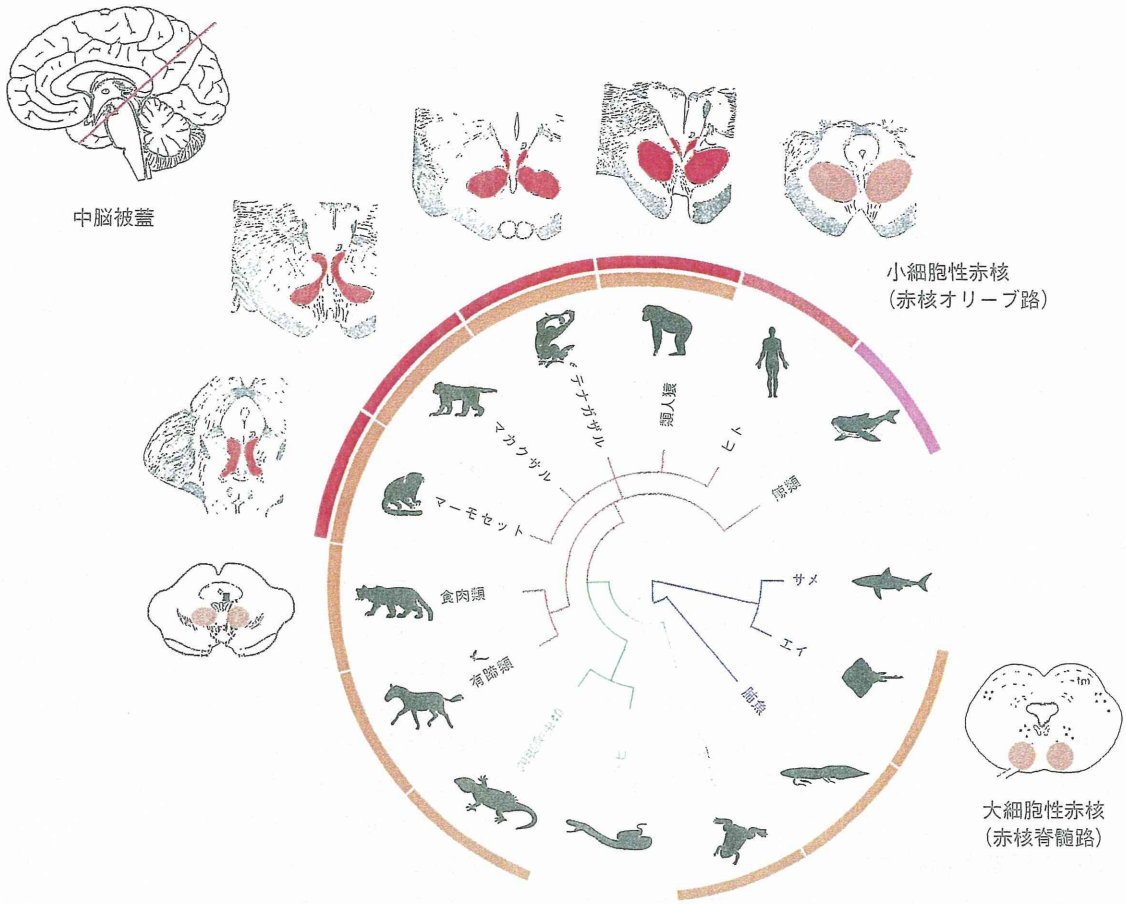

Fig. 1　赤核の系統発生と比較解剖（大細胞性赤核と小細胞性赤核）
橙：大細胞性赤核．赤：小細胞性赤核．大細胞性赤核は四肢による locomotion を行う脊椎動物で発達している．小細胞性赤核は霊長類の発達に特徴的である（被蓋断面図は井口[6]，ten Donkelaar[7]を改変）．

である．その中で，赤核の発達の程度は脊椎動物の系統発生の過程，つまり対鰭（ヒレ）から肢への系統発生の過程と一致していることが多くの研究者を惹きつけた（**Fig. 1**）．赤核脊髄路は古代に分岐した軟骨魚類（サメなど）の中でもエイには存在し，さらに硬骨魚類とは異なり，発達した内骨格，つまり肢の原型を有する肉鰭類（シーラカンスなど）や両生類（カエルなど）はより発達する．このように赤核脊髄路は，ヒレないし肢をロコモーションに使う脊椎動物において発達し，その発達の度合はヒレから肢へと四肢の構造の発達の度合と比例している[7,8]．さらに爬虫類，哺乳類において陸生となり歩行，走行など四肢の制御様式がより発達するようになると，赤核，赤核脊髄路も相対的に大きくなり，それにかかわる神経回路も徐々に複雑になる．つまり赤核は水中から陸上への適応の過程において，最も重要であった四肢の発達と並行に，文字通り「歩みをともにしてきた」神経核なのである．このような比較神経解剖学的な見地から，赤核は赤核脊髄路を介して四肢歩行において重要な役割

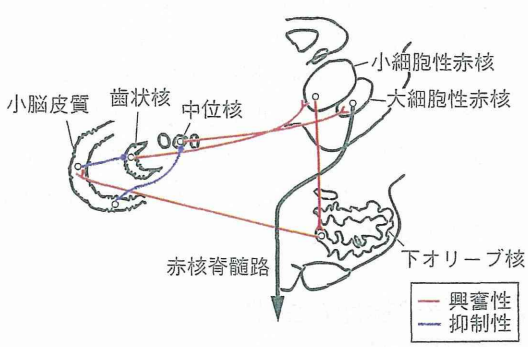

Fig. 2　赤核-オリーブ-小脳の回路図
大細胞性赤核の軸索は延髄にて交叉し，対側の脊髄へ投射する赤核脊髄路を形成する．一方，小細胞性赤核は同側の下オリーブ核へ投射し（中心被蓋路），下オリーブ核からは対側の小脳皮質へ登上線維を出す．小脳皮質プルキンエ細胞は深部の出力核へ抑制性の入力を送る．小脳深部核は上小脳脚を介して対側の赤核へ（大細胞性へは中位核から，小細胞性は歯状核から）興奮性の入力をもたらす．小細胞性赤核-下オリーブ核-小脳の成す再帰性ループを一般に「小川の三角形」と呼ぶ．

を果たすことが推察されており，進化，発生的な観点からも興味深い研究対象である．

2．2つの赤核

赤核脊髄路の起始となる神経細胞は，大きな細胞体をもつことから大細胞性赤核と呼ばれ，より尾側に位置する．一方，霊長類において発達を遂げたのは多数の小さな細胞からなる小細胞性赤核と呼ばれる部位で，大細胞性より吻側に位置する．小細胞性赤核は霊長類の中でも系統発生においてヒトに近くなるにつれて顕著に発達している．こうした区分の違いは細胞の大小だけではなく，連絡する回路に関しても大きな違いがある．

1 大細胞性赤核と赤核脊髄路

大細胞性赤核の線維連絡に関して（**Fig. 2**），入力においては小脳の深部にある中位核から最も強力な興奮性の入力を受ける．また大脳皮質4野などの運動関連野からの入力を受ける[10]．さらに，末梢からは脊髄の屈曲反射介在ニューロンからの入力も受ける[11]．出力は赤核脊髄路として延髄にて対側へ交叉し，皮質脊髄路と平行して背側索を下行し脊髄へと至る．また一部の軸索は外側網様体などの延髄の核に投射する．

2 小細胞性赤核と赤核オリーブ路

小細胞性赤核は小脳の歯状核から入力を受ける．歯状核は小脳の深部出力核のうちで最も外側にあり，系統発生的な観点から最も新しい核である．また小細胞性赤核は大脳皮質のうち4野，5野，6野，24野などからの入力を受ける[10]．小細胞性赤核の細胞のほぼすべてが下オリーブ核へ出力する（赤核オリーブ路）．下オリーブ核は登上線維を介して小脳皮質へ連絡するため，小脳歯状核-赤核-下オリーブ核は再帰性回路を形成し，これは本邦ではその存在を初めて認めた小川鼎三の名にちなみ「小川の三角形」，国外では「Guillain-Mollaret triangle」とも呼ばれる（**Fig. 2**）．

3．赤核の機能と生理

1 赤核脊髄路

上記のようにその細胞構築，形成する回路の観点から赤核は2つに区分されるが，動物を用いた実験によって精力的にその生理機能が調べられてきたのはおもに大細胞性赤核，赤核脊髄路細胞である．赤核脊髄路の生理作用については，1960年代からのLundberg，本郷らによる一連の研究により詳細が明らかにされた[12~15]．そこでは，実験動物としてネコを対象に，電気刺激や細胞内記録を組み合わせた実験が行われた．

大細胞性赤核由来の軸索はおもに脊髄内中間層（RexedのⅥ，Ⅶ層）に終止し，脊髄介在ニューロンを介して間接的にアルファ運動ニューロンに作用を及ぼす．これにより単シナプス性に興奮させられる脊髄介在ニューロンには，筋紡錘（Ⅰa群求心線維）とGolgi腱器官（Ⅰb群求心線維）から単シナプス性興奮性入力を受けるもの，これから2シナプス性抑制入力を受けるもの，また，屈曲反射を起こす求心性線維から興奮性入力を受けるものがあり，これらの介在ニューロンを介して，屈筋を支配するアルファ運動ニューロンに対してはおもに促通作用を及ぼし，伸筋を支配するアルファ運動ニューロンに対してはおもに抑制作用を及ぼす相反性を特徴とする．また一部の細胞は直接アルファ運動ニューロン，ガンマ運動ニューロン，とりわけ動的ガンマ運動ニューロンに単シナプス性興奮作用を及ぼす．さらに，動的ガンマ運動ニューロンに対する作用には相反関係がみられ，屈筋を支配する動的ガンマ運動ニューロンの活動を亢進させるとともに，伸筋のそれを抑制する．このように脊髄内における回路結合を総合すると，大細胞性赤核は赤核脊髄路を介して伸筋-屈筋の相反抑制支配に関して，Ⅰa，Ⅰb反射およびアルファ-ガンマ連関などの相反性の回路と，屈曲反射の系を利用して，関節の屈曲運動を円滑に行っている系だと考えられる．

このような赤核脊髄路ニューロンが，おもに小脳から制御されているということはToyamaら[16]の急性標本，さらには除脳ネコの標本によって明らかにされてきた．歩行中において遊脚相や前肢を前に出す動作など，屈筋が活動しているときに大細胞性赤核の活動は増大するが，上小脳脚の離断した標本においてはその活動の変化が完全に消失することや[17]，小脳皮質冷却による小脳中位核の脱抑制による過活動に伴い，大細胞性赤核も過活動すること[18]，その際には過屈曲が起こることなどから[19]，小脳の屈曲出力機構であることが示されている．さらには障害物を乗り越えるときや[20]，屈筋を用いてパターンの補正または遊脚相の前肢振り出し運動を発展させたような到達運動において活動が上がるという実験結果もこの考えを支持している[21]．

同様な結果は，覚醒行動中のマカクザルを対象とした研究においても示されている．たとえば，バイクのスロットルを握って回すような動作をサルに行わせると，大細胞性赤核の細胞活動は最大の発火頻度を示す[22]．また，目標物に向かって腕を伸ばして把握するという一連の到達把握運動においても，物体把握の直前，手首を伸展（ネコなど四肢動物においては屈曲となる：生理学的屈曲）させるときにその発火頻度が急激に増加することが知られている[23]．さらに，スパイク加算平均法によって

赤核脊髄路細胞と筋における機能的シナプス結合の定量的評価を行った研究によっても，大細胞性赤核から屈筋への結合のほうが，伸筋へのそれに比較して数，強度においても優性であることが明らかにされた[24]．筆者らの実験においても同様に，上肢の多様な運動中の記録された赤核脊髄路細胞から筋への機能的結合のグループは，それぞれ肩，肘，手首，指の生理学的屈筋群が動員されて，到達運動の協調にかかわっていることが示唆されている[25]．

このように，赤核脊髄路，大細胞性赤核は小脳が適応的に運動を制御する際の出力機構として，とりわけ肢を折りたたむ（屈曲）運動を惹起する機能を有していることが今までの研究から強く示唆されている．四肢動物は，おそらくこの小脳-赤核機構を通じて屈曲反射や腱反射などの反射回路を適切に調節することにより歩行のサイクルを調整し，体の姿勢を安定的に維持しつつ高速移動を実現していると考えられる．実際，齧歯類標本において，薬理ブロックによる大細胞性赤核の神経活動の不活化により歩行時の床反力の異常がみられることから[26]，歩行中接地時の衝撃を和らげるダンパーとしての機能を調節していることが示唆されている．他方，四肢歩行から樹上へと環境を移した霊長類においては，そうした適応的屈曲機構を，上肢の到達運動中の把握の準備動作へと転用（外適応）しているのだと解釈することも可能であろう．

しかしながら，この赤核脊髄路は，ヒトにおいてはかなり退化，萎縮していることがモナコフの発見以後再三指摘され続けており[5,9]，上記の機能を十分に果たすことができるとは考えにくい．このため，ネコやサルなどの実験動物を対象に得られた知見を，ヒトの神経系の機能や病態に結びつけることは困難を伴う．

2 小細胞性赤核の機能，損傷による病態

これまで述べた通り，小細胞性赤核は霊長類，特にヒトにおいて顕著な発達したと考えられるが，その機能に関してはいまだに解明されておらず，その解明に取り組む研究も多くない．一方で，赤核症候群と呼ばれる赤核に病変がある際に発現する病態が古くからおもにフランスで蓄積され，損傷実験による同症状のモデル動物としてのサルが実験的に再現されている．ここでは，これらの研究成果を紹介し，小細胞性赤核を含む回路の異常に起因する障害について概説する．

1）ヒトにおける赤核障害

赤核の病変とそれに伴うおもに運動障害は赤核症候群と呼ばれ，歴史的変遷に伴い Benedikt 症候群[27,28]，Claude 症候群[29]などを含み，多様な臨床病態を示す[30]．

Benedikt 症候群とは，腫瘍（おもに結核腫）と血管障害（軟化巣）が原因となり一側赤核部位や，そこを通過する上小脳脚の障害に起因する．それによって，同側の動眼神経麻痺と反対側の半身に不全麻痺が起こり，同じく反対側の上下肢に振戦，ないし舞踏病，アテトーゼ様の自発性不随意運動がみられるものをいう．不随意運動の性質は多様で一定しないが，企図運動に際して増強する性質をもつ．Claude 症候群とは，1912 年に Claude が報告したもので[29]，一側の動眼神経麻痺と対側の上下肢の運動失調など，いわゆる小脳症状を呈し，筋緊張亢進と自発性不随意運動はなく，病変は赤核とともに，上小脳脚が赤核に終止する所で強く認められる．実際のところ赤核症候群の分類に関して境界は曖昧であり[30]，おそらくは神経核，終始する線維，または通過線維などの損傷の度合によるものだろうと推察されている．しかしながら頻繁にみられる症状として，対側の不随意運動や運動失調，そして振戦が挙げられる．

赤核障害による振戦（赤核振戦）に関しては，Holmes[31]によって詳細にまとめられた．一側上肢主体で，拮抗筋との間で交代性収縮を示し，緩徐（3～5 Hz），規則的かつ粗大であり，安静時にも出現するが，企図振戦を伴い，また姿勢の維持によって増強する．また四肢だけでなく，舌咽頭の振戦ともいうべき口蓋ミオクロニーの原因になる神経回路として小脳歯状核-赤核-オリーブ核-小脳，つまり「小川の三角形」が関与しており，振戦の発現に小細胞性赤核が何らかの関係があることが示唆されてきた．

2）赤核モデル動物の作出

これらの臨床病態をもとに小川ら[5,32]は，ウサギ，イヌ，ネコの小細胞性赤核と赤核オリーブ路を含む中心被蓋路の破壊を含む比較解剖学的実験を積み重ね，サルを用いて一側小細胞性赤核ないしこれより下行する中心被蓋路の破壊を行い，①顎が破壊側に向かう型の斜頚と，②反対側の半身不全麻痺と企図振戦，運動失調を呈する動物を作出し，Benedikt 症候群，Claude 症候群などを再現した．

大江らは振戦の発現機構としての赤核障害に注目し，脳室造影による脳深部の位置の推定と，微小電極による細胞の自発発射記録を組み合わせることで赤核破壊をより高精度で行う方法を確立し，サルを対象とした実験においてそれを用いた．そして赤核近辺で考えられる振戦発現の経路，つまり①黒質-線条体路，②小細胞性赤核-オリーブ路および，③小脳-視床路の 3 つの代表的経路を経時的にそれぞれ順番に破壊し，その順番を問わず，この 3 つの経路がすべて破壊されることがサルの振戦

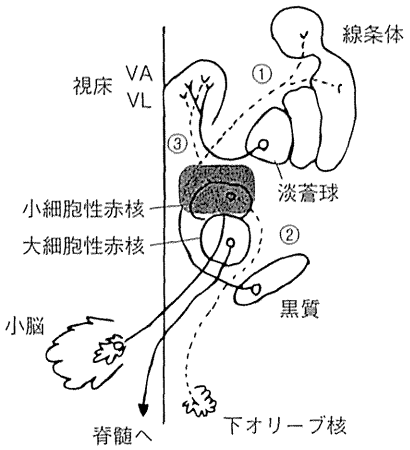

Fig. 3　振戦発現の障害部位
中脳被蓋腹側部の破壊(グレーのエリア)により振戦が起きる際に，障害される責任経路を点線で示す．①黒質-線条体路，②小細胞性赤核-オリーブ路および，③小脳-視床路．(大江[4]を改変)

発現に必要な条件であることを発見した[3,4](**Fig. 3**)．自発性振戦がよく発現した例の破壊巣はすべて，小細胞性赤核の70%以上と，黒質細胞の70%以上が障害されていたという．大江らはさらに，この自発性振戦の出現しているサルを用いて，振戦を伝達する脊髄への下行路として，皮質脊髄路（脊髄側索）ではなく橋網様体から脊髄前索を下行する網様体脊髄路が責任経路だと論じている[33]．Imai ら[34,35]はさらに薬理学的に破壊する方法を用いて，軽度ながら痙性斜頸や対側上肢の安静時振戦などを惹き起こす振戦モデルサルの作出に成功している．

このように小細胞性赤核は，大脳基底核や脳幹のほかの部位と連関し，不随意運動や振戦などに何らかのかかわりをもつことが臨床病態，破壊実験などにより明らかにされてきたが，その機序に関してはいまだ不明である．

4．赤核研究における今後の展望

以上のように，大細胞性と小細胞性赤核細胞によって構成される神経回路は異なっているが，両者とも小脳から強力な入力を受けて，出力する核という共通点をもつ．また，大細胞性赤核は楔状束核を介して下オリーブ核の細胞に抑制性の入力作用をもつことが示されており[36]，間接的，直接的の違いはあるものの下オリーブ核への入力をもつという点で一致する．したがって，赤核の機能の本質は下オリーブ核に作用して小脳への入力に何らかの変化をもたらす，つまり小脳-赤核-オリーブ核が形成する再帰性回路（小川の三角形）に由来する機能であると考えられる．そして，この機能が障害されると，霊長類の場合運動系の発振としての振戦や，多様な不随意運動が起こる．本稿で紹介したこのような知見は，ほとんどが20世紀の間に確立したものである．近年急速に発展しつつある遺伝学を応用した回路特異的な操作，介入する手法を用いて，赤核の機能や赤核障害に伴う運動不全の機序を調べ，運動制御における赤核の機能を再検討すべき時期がきていると，著者らは考えている．

文　献

1) 山下勝幸：赤核脊髄路．*Clin Neurosci* **27**：742-745，2009
2) 今井壽正：振戦発現機構の分析と治療．神研の進歩 **34**，976-985，1990
3) 大江千廣：赤核症候群．現代医療 **11**：787-789，1979
4) 大江千廣：振戦の神経機序．神研の進歩 **25**：106-117，1981
5) 小川鼎三：脳の解剖学．東京，南山堂，1951，pp76-106
6) 井口 巌：霊長類の赤核に関する比較解剖学的研究．解剖学雑誌 **23**：1-3，1946
7) ten Donkelaar HJ：Evolution of the red nucleus and rubrospinal tract. *Behav Brain Res* **28**：9-20，1988
8) Massion J：The mammalian red nucleus. *Physiol Rev* **47**：383-436，1967
9) Nathan PW，Smith MC：The rubrospinal and central tegmental tracts in man. *Brain* **105**：223-269，1982
10) Burman K，Darian-Smith C，Darian-Smith I：Geometry of rubrospinal，rubroolivary，and local circuit neurons in the macaque red nucleus. *J Comp Neurol* **423**：197-219，2000
11) Padel Y，Bourbonnais D，Sybirska E：A new pathway from primary afferents to the red nucleus. *Neurosci Lett* **64**：75-80，1986
12) Hongo T，Jankowska E，Lundberg A：The rubrospinal tract. Ⅰ. Effects on alpha-motoneurones innervating hindlimb muscles in cats. *Exp Brain Res* **7**：344-364，1969
13) Hongo T，Jankowska E，Lundberg A：The rubrospinal tract. Ⅱ. Facilitation of interneuronal transmission in reflex paths to motoneurones. *Exp Brain Res* **7**：365-391，1969
14) Hongo T，Jankowska E，Lundberg A：The rubrospinal tract. Ⅲ. Effects on primary afferent terminals. *Exp Brain Res* **15**：39-53，1972
15) Hongo T，Jankowska E，Lundberg A：The rubrospinal tract. Ⅳ. Effects on interneurones. *Exp Brain Res* **15**：54-78，1972
16) Toyama K，Tsukahara N，Udo M：Nature of the cerebellar influences upon the red nucleus neurones. *Exp Brain Res* **4**：292-309，1968
17) Orlovsky GN：Activity of rubrospinal neurons during locomotion. *Brain Res* **46**：99-112，1972
18) Udo M，Matsukawa K，Kamei H：Effects of partial cooling of cerebellar cortex at lobules Ⅴ and Ⅳ of the intermediate part in the decerebrate walking cats under monitoring vertical floor reaction forces. *Brain Res* **160**：559-564，1979
19) Udo M，Matsukawa K，Kamei H：Hyperflexion and changes in interlimb coordination of locomotion induced by cooling of the cerebellar intermediate cortex in normal cats. *Brain Res* **166**：405-408，1979
20) Zelenin PV，Beloozerova IN，Sirota MG，et al：Activity of red nucleus neurons in the cat during postural corrections. *J Neurosci* **30**：14533-14542，2010
21) Lavoie S，Drew T：Discharge characteristics of neurons in the red nucleus during voluntary gait modifications：a comparison with the motor cortex. *J Neurophysiol* **88**：1791-1814，2002
22) Gibson AR，Houk JC，Kohlerman NJ：Magnocellular red nucleus activity during different types of limb movement in the macaque monkey. *J Physiol* **358**：527-549，1985

23) van Kan PL, McCurdy ML : Role of primate magnocellular red nucleus neurons in controlling hand preshaping during reaching to grasp. *J Neurophysiol* **85** : 1461-1478, 2001
24) Cheney PD, Mewes K, Widener G : Effects on wrist and digit muscle activity from microstimuli applied at the sites of rubromotoneuronal cells in primates. *J Neurophysiol* **66** : 1978-1992, 1991
25) 大屋知徹，武井智彦，関　和彦：赤核の機能と回路における推察．Motor Control 研究会要旨，2014
26) Muir GD, Whishaw IQ : Red nucleus lesions impair overground locomotion in rats : a kinetic analysis. *Eur J Neurosci* **12** : 1113-1122, 2000
27) Benedikt M : Nervenpathologie Und Elektrotherapie. Leipzig, Fues's Verlag, 1874, pp311-312
28) Benedikt M : Tremblement avec paralyse croisée du moteur oculaire commun. *Bulletin Medical* **3** : 547-548, 1889
29) Claude H : Syndrome péduncuIaire de la region du noyau rouge. *Rev Neurol* **23** : 311-313, 1912
30) Souques M, Crouzon M, Bertrand I : Révision du syndrome de Benedikt. Á propos de l'autopsie d'un cas de ce syndrome. Forme trémo-choréo-athétoïde et hypertonique du syndrome du noyau rouge. *Rev Neurol Tom* II : 377-417, 1930
31) Holmes G : On certain tremors in organic cerebral lesions. *Brain* **27** : 327-375, 1904
32) 小川鼎三，佐野文男：クラーク氏装置による猿の中脳被蓋破壊実験．解剖学雑誌 **20** : 437-472, 1942
33) Ohye C, Shibazaki T, Hirai Y, et al : Possible descending pathways mediating spontaneous tremor in monkeys. *Adv Neurol* **40** : 181-188, 1984
34) Imai H, Nakazato T, Narabayashi H : Motor symptoms in the monkey with unilateral injection of kainic acid into the red nucleus and systemic injection of MPTP. *Neurosci Res Suppl* **5** : 48, 1987
35) Imai H, Nakamura T, Endo K, et al : Hemiparkinsonism in monkeys after unilateral caudate nucleus infusion of 1-methyl-4-phenyl-1,2,3,6-tetrahydropyridine (MPTP) : behavior and histology. *Brain Res* **474** : 327-332, 1988
36) Horn KM, Hamm TM, Gibson AR : Red nucleus stimulation inhibits within the inferior olive. *J Neurophysiol* **80** : 3127-3136, 1998

THE JOURNAL OF BIOLOGICAL CHEMISTRY VOL. 290, NO. 3, pp. 1442–1453, January 16, 2015

p62 Plays a Protective Role in the Autophagic Degradation of Polyglutamine Protein Oligomers in Polyglutamine Disease Model Flies*

Received for publication, June 20, 2014, and in revised form, November 26, 2014 Published, JBC Papers in Press, December 5, 2014, DOI 10.1074/jbc.M114.590281

Yuji Saitoh[‡§¶], Nobuhiro Fujikake[‡], Yuma Okamoto[‡], H. Akiko Popiel[‡], Yusuke Hatanaka[‡], Morio Ueyama[‡], Mari Suzuki[‡], Sébastien Gaumer[‖], Miho Murata[§¶], Keiji Wada[‡], and Yoshitaka Nagai[‡1]**

*From the [‡]Department of Degenerative Neurological Diseases, National Institute of Neuroscience, National Center of Neurology and Psychiatry, 4-1-1 Ogawa-Higashi, Kodaira, Tokyo 187-8502, Japan, the [§]Department of Neurology, National Center Hospital, National Center of Neurology and Psychiatry, 4-1-1 Ogawa-higashi, Kodaira, Tokyo 187-8551, Japan, the [¶]Graduate School of Medical and Pharmaceutical Sciences, Chiba University, 1-8-1, Inohana, Chuo-ku, Chiba, Chiba 260-8670, Japan, the [‖]Laboratoire de Génétique et Biologie Cellulaire, EA4589, Université de Versailles-Saint-Quentin-en-Yvelines, École Pratique des Hautes Etudes, 45 Avenue des Etats-Unis, 78035 Versailles Cedex, France, and **Core Research for Evolutional Science and Technology (CREST), Japan Science and Technology Agency, Kawaguchi, Saitama 332-0012, Japan*

Background: Oligomers of pathogenic proteins are implicated in the pathomechanisms of neurodegenerative diseases.
Results: Depletion of p62 delays the degradation of polyglutamine protein oligomers via autophagy and exacerbates neurodegeneration in polyglutamine disease model flies.
Conclusion: p62 plays a protective role via autophagic degradation of polyglutamine protein oligomers.
Significance: p62 should be a therapeutic target for the polyglutamine diseases.

Oligomer formation and accumulation of pathogenic proteins are key events in the pathomechanisms of many neurodegenerative diseases, such as Alzheimer disease, ALS, and the polyglutamine (polyQ) diseases. The autophagy-lysosome degradation system may have therapeutic potential against these diseases because it can degrade even large oligomers. Although p62/sequestosome 1 plays a physiological role in selective autophagy of ubiquitinated proteins, whether p62 recognizes and degrades pathogenic proteins in neurodegenerative diseases has remained unclear. In this study, to elucidate the role of p62 in such pathogenic conditions *in vivo*, we used *Drosophila* models of neurodegenerative diseases. We found that p62 predominantly co-localizes with cytoplasmic polyQ protein aggregates in the MJDtr-Q78 polyQ disease model flies. Loss of p62 function resulted in significant exacerbation of eye degeneration in these flies. Immunohistochemical analyses revealed enhanced accumulation of cytoplasmic aggregates by *p62* knockdown in the MJDtr-Q78 flies, similarly to knockdown of autophagy-related genes (*Atgs*). Knockdown of both *p62* and *Atgs* did not show any additive effects in the MJDtr-Q78 flies, implying that p62 function is mediated by autophagy. Biochemical analyses showed that loss of p62 function delays the degradation of the MJDtr-Q78 protein, especially its oligomeric species. We also found that loss of p62 function exacerbates eye degeneration in another polyQ disease fly model as well as in ALS model flies. We therefore conclude that p62 plays a protective role against polyQ-induced neurodegeneration, by the autophagic degradation of polyQ protein oligomers *in vivo*, indicating its therapeutic potential for the polyQ diseases and possibly for other neurodegenerative diseases.

The polyglutamine (polyQ)[2] diseases are inherited intractable neurodegenerative diseases, including Huntington disease, several spinocerebellar ataxias (SCA1, -2, -6, -7, and -17 and SCA3/MJD), dentatorubral-pallidoluysian atrophy, and spinobulbar muscular atrophy, which are caused by the expansion of a CAG repeat encoding for polyQ stretch within specific genes (1). PolyQ proteins are prone to misfold, oligomerize, and form aggregates and eventually accumulate as inclusion bodies in affected neurons (2, 3). Whereas the formation of polyQ protein inclusion bodies is believed to be protective, by sequestering the toxic polyQ proteins (4), the intermediate structures formed during the aggregation process, such as monomers or oligomers, are reported to be more toxic for the cells, leading to neuronal dysfunction or neuronal cell death (5, 6). The polyQ diseases are thus considered as one of the protein-folding diseases, together with Alzheimer disease, Parkinson disease, and ALS. Because there are currently no effective therapies for the polyQ diseases, establishment of a novel therapy based on the

* This work was supported in part by Grants-in-Aid for Scientific Research (B) (to Y. N.) from the Japan Society for the Promotion of Science (JSPS), Japan; by Grants-in-Aid for Scientific Research on Priority Areas (Proteolysis) (to Y. N.) and on Innovative Areas (Synapse and Neurocircuit Pathology) (to Y. N.) from the Ministry of Education, Culture, Sports, Science, and Technology, Japan; by Health Labor Sciences Research Grants for Research on Development of New Drugs and the Research Committee for Ataxic Diseases (to Y. N.) from the Ministry of Health, Labor, and Welfare, Japan; and by a grant from Core Research for Evolutional Science and Technology (CREST) of the Japan Science and Technology Agency (to Y. N.).

[1] To whom correspondence should be addressed: Dept. of Degenerative Neurological Diseases, National Institute of Neuroscience, National Center of Neurology and Psychiatry, 4-1-1 Ogawa-Higashi, Kodaira, Tokyo 187-8502, Japan. Tel.: 81-42-346-1715; Fax 81-42-346-1745; E-mail: nagai@ncnp.go.jp.

[2] The abbreviations used are: polyQ, polyglutamine; UPS, ubiquitin-proteasome system; MJDtr, truncated form of mutant MJD; IR, inverted repeat RNA; Aβ, amyloid-β; AGE, agarose gel electrophoresis; SEM, scanning electron microscopic.

disease pathomechanism is a challenging theme. Considering the pathomechanism of the polyQ diseases, the clearance of toxic forms of the polyQ proteins should be a promising therapeutic strategy.

Although the precise mechanisms of how polyQ proteins are degraded in the cell are not clearly understood, the two major cellular degradation systems (*i.e.* the autophagy-lysosome system and the ubiquitin-proteasome system (UPS)) are both thought to be involved in polyQ protein degradation (7). However, the UPS may be inadequate for degrading polyQ protein oligomers or aggregates, because substrate proteins of the UPS need to be unfolded when entering the narrow proteasomal pore (8). Furthermore, the mammalian UPS might not have a protease activity to efficiently degrade the polyQ stretch (9, 10). Alternatively, autophagy can degrade even large aggregates by sequestering and delivering them to the lysosome (11). Although autophagy was considered a non-selective degradation system in the past, emerging evidence suggests that it can specifically degrade some ubiquitinated proteins, organelles, and intracellular pathogens; this is now known as "selective autophagy" (12). The specific autophagic degradation of polyQ proteins, including large sized aggregates, would be a preferable therapeutic strategy, because nonspecific degradation of cytosolic proteins may cause adverse effects due to the loss of normal protein functions.

The p62/sequestosome 1 protein (hereafter called p62) was initially identified as an adaptor molecule for the selective autophagic degradation of ubiquitinated proteins, because p62 has domains that bind both ubiquitinated proteins and autophagosomes, giving selectivity to autophagy (13, 14). Neuropathological studies revealed that p62 co-localizes with ubiquitin-positive inclusions consisting of disease-causative proteins within neurons and glia of patients with various neurodegenerative diseases (15, 16). This evidence suggests that p62 is associated with various abnormal proteins, including the polyQ protein. However, whether p62 recognizes these pathogenic proteins as substrates for p62-associated selective autophagy has remained unclear.

In this study, we explored the role of p62 in the polyQ diseases, using *Drosophila* polyQ disease models. We demonstrated that p62 plays an important role in the autophagic degradation of polyQ protein oligomers, resulting in protection against polyQ protein toxicity *in vivo*. Furthermore, we demonstrated the protective role of p62 in various neurodegenerative disease models, indicating that p62 could be a therapeutic target for various neurodegenerative diseases.

EXPERIMENTAL PROCEDURES

Fly Stocks—Flies were raised and maintained on standard cornmeal-agar-yeast-based food at 25 °C. The transgenic fly lines bearing the *gmr-GAL4* (17) or *UAS*-human *TDP-43*[3] transgene have been described previously. The transgenic fly lines bearing the *gmr-GeneSwitch* or *gmr-grim* transgene and the mutant fly line bearing the $Atg6^{00096}$ mutation were obtained from the Bloomington *Drosophila* Stock Center. The transgenic fly lines bearing the *UAS-MJDtr-Q78* and *UAS-MJDtr-Q27* transgene were gifts from Drs. N. M. Bonini (18), and the *UAS-Httex1p97QP* (19), *UAS-Aβ arc2* (20), and *UAS-R406W tau* (21) transgene were gifts from J. L. Marsh, D. C. Crowther, and M. B. Feany, respectively. The mutant fly lines bearing a *ref(2)P* mutation, namely $ref(2)P^{od42}$ or $ref(2)P^{od3}$, were described previously (22). The RNAi fly lines bearing the *UAS-ref(2)P-IR*, *UAS-Atg12-IR*, *UAS-alfy-IR*, or *UAS-Prosβ2-IR* transgene were obtained from the Vienna *Drosophila* Resource Center.

Fly Eye Imaging—Light microscopic images were taken using a stereoscopic microscope model SZX10 (Olympus, Tokyo, Japan) with a CCD camera (PD21, Olympus, Tokyo, Japan). Scanning electron microscopic (SEM) images were taken using an electron microscope (model TM1000, Hitachi, Tokyo, Japan).

Calculation of Eye Pigmentation Score—The eye images of adult flies were obtained. To quantitatively evaluate the degree of eye degeneration in the MJDtr-Q78 flies, the area of remaining normal pigment in their eyes were measured using the National Institutes of Health ImageJ software as follows: 1) extraction of the green color to produce grayscale images and determination of the area of compound eye as the region of interest (Fig. 2, *Q* and *R*); 2) smoothing of the images by Gaussian blur (Fig. 2*S*), production of binary images, and adjustment of the threshold of the binary images to determine the area of remaining normal pigment in the eyes (Fig. 2*T*); and 3) calculation of the mean area of remaining normal pigment within the region of interest. For the TDP-43 flies, the region of interest was determined in the anterior half of the eye to avoid the necrotic tissues appeared in the posterior half because the necrotic tissues could be misjudged as normal pigment. More than four eyes were analyzed in each experiment.

Calculation of the Number of Interommatidial Bristles—The SEM images of adult fly eyes were obtained. The number of interommatidial bristles within a 150-μm^2 area in the eye was counted (23). Seven eyes were analyzed in each genotype.

Calculation of Eye Size—The light microscopic images of adult fly eyes were obtained. The eye size was measured using ImageJ software (24). Ten eyes were analyzed in each genotype.

Immunohistochemistry—Eye discs were dissected from third instar larvae, fixed with 4% paraformaldehyde, and then immunostained with a rat monoclonal anti-HA antibody (clone 3F10, Roche Applied Science), a rabbit polyclonal anti-Ref(2)P/p62 protein antibody (22), or a mouse monoclonal anti-elav antibody (clone 9F8A9, Developmental Studies Hybridoma Bank, Iowa City, IA) at 1:200 dilution as the primary antibody. As the secondary antibody, an Alexa 568-conjugated anti-rat antibody, an Alexa 488-conjugated anti-rabbit antibody, or an Alexa 488-conjugated anti-mouse antibody was used at 1:1000 dilution. Nuclei were stained using DAPI (Bio-Rad) after the secondary antibody staining. An Alexa 647-conjugated wheat germ agglutinin (Molecular Probes, Inc., Eugene, OR) staining to define the nuclear membrane was performed after DAPI staining at 1:500 dilution. Images were then taken by confocal laser-scanning microscopy (FV1000, Olympus, Tokyo, Japan).

[3] N. Fujikake, N. Kimura, Y. Saitoh, S. Nagano, Y. Hatanaka, T. Ishiguro, T. Takeuchi, M. Suzuki, H. A. Popiel, E. N. Minakawa, M. Ueyama, G. Matsumoto, A. Yokoseki, N. Nukina, T. Araki, O. Onodera, K. Wada, and Y. Nagai, submitted for publication.

The number of MJDtr-Q78 protein aggregates in the eye discs was quantitatively measured using the FV10-ASW 2.0 Viewer software (Olympus, Tokyo, Japan), as follows: 1) selection of photoreceptor neurons within the 13 developing ommatidia in row 2 and row 3 at the posterior tip of the eye discs, by anti-elav staining (Fig. 4, *E* and *F*), because these ommatidia are in approximately the same developing stage and can be easily identified; 2) counting of the number of MJDtr-Q78 protein aggregates localized in either the cytoplasm or the nucleus, judged by whether they merge with the nuclei stained with DAPI or not (Fig. 4, *G* and *H*). More than five eye discs were analyzed in each experiment.

Western Blot Analysis—Five heads of adult flies or 20 eye discs of larvae were lysed in 100 μl of SDS sample buffer using a pestle, sonicated, boiled for 5 min, and centrifuged at 10,000 × *g* for 3 min at 25 °C. The supernatants were run on a 5–20% gradient polyacrylamide gel (Wako, Osaka, Japan) and then transferred onto an Immun-Blot PVDF membrane (Bio-Rad). The membrane was blocked with 5% skim milk in PBS containing 0.1% Tween 20 for 30 min at room temperature and then incubated overnight with a rat monoclonal anti-HA antibody (clone 3F10, Roche Applied Science), a rabbit polyclonal anti-Ref(2)P/p62 antibody (22), or a mouse monoclonal anti-actin antibody (clone AC-40, Sigma-Aldrich) at 1:1000 dilution as primary antibody. After overnight incubation, the membranes were incubated with HRP-conjugated secondary antibodies. Membranes were then treated with SuperSignal West Dura chemiluminescent substrate (Thermo Fisher Scientific), and images were taken by the LAS-4000 imaging system (Fujifilm, Tokyo, Japan). Quantification of each signal was performed using the MultiGauge software (Fujifilm).

SDS-Agarose Gel Electrophoresis (SDS-AGE)—SDS-AGE was performed according to the previous reports (25–27). Briefly, adult fly head lysates were run on a 1.5% agarose, 0.1% SDS gel and then transferred onto a nitrocellulose membrane (Schleicher & Schuell BioScience). Blocking with skim milk, reaction with the primary or secondary antibody, and detection were done with the same protocols as Western blot analysis.

Gene Switch Protocol—RU486 (mifepristone, Sigma-Aldrich) was dissolved in 100% ethanol, further diluted in water, and then mixed with Instant *Drosophila* medium at a final concentration of 10 μg/ml (Carolina Biological Supply Company, Burlington, NC). For RU486 treatment, flies were in RU486-containing medium from the larval stage until adulthood.

Statistical Analyses—For comparisons between two groups, statistical differences were analyzed by Student's *t* test. Data are presented as the mean ± S.E. A p value of <0.05 was considered to indicate a statistically significant difference between groups.

RESULTS

p62 Co-localizes with Cytoplasmic PolyQ Protein Aggregates—To evaluate whether p62 affects the polyQ protein *in vivo*, we used the MJDtr-Q78S transgenic fly line, which expresses a truncated form of the mutant MJD protein with an expanded Gln-78 repeat (MJDtr-Q78). As a control, we used the MJDtr-Q27 transgenic fly line, which expresses a truncated form of the MJD protein with a normal-length Gln-27 repeat (MJDtr-Q27). The MJDtr-Q78S flies showed severe compound eye degeneration when the MJDtr-Q78 protein was selectively expressed in the eye by the *gmr-GAL4* driver, as revealed by light microscopic analyses (18) (Fig. 1*B*). On the contrary, the MJDtr-Q27 flies did not show any eye degenerative phenotypes (Fig. 1*A*). In these MJDtr-Q78S flies, the MJDtr-Q78 protein was found to accumulate as aggregates in both the cytoplasm and nucleus, although nuclear aggregates were more abundant than cytoplasmic aggregates (Fig. 1, *I* and *J*). To evaluate the relationship between p62 and the MJDtr-Q78 protein, we performed immunohistochemical analyses of larval eye discs. In the MJDtr-Q27 flies, p62 was predominantly present in the cytoplasm (Fig. 1, *C–H*), and punctate dotlike structures were also observed, which are known as "p62 bodies" (28) (Fig. 1*F*, *open arrows*). On the other hand, in the MJDtr-Q78S flies, p62 co-localized with cytoplasmic MJDtr-Q78 protein aggregates but not with nuclear aggregates (Fig. 1, *I–N*), although most MJDtr-Q78 protein aggregates were present in the nucleus. Wheat germ agglutinin staining to define the nuclear membrane revealed that p62-positive MJDtr-Q78 protein aggregates are present in the cytoplasm, and p62-negative MJDtr-Q78 protein aggregates are present in the nucleus (Fig. 1, *O–Q*). The size of p62-positive MJDtr-Q78 protein aggregates was much larger than that of the p62 bodies seen in the control flies, indicating that these p62-positive MJDtr-Q78 protein aggregates are different from the p62 bodies (Fig. 1, *F* and *L*). These results suggest that p62 is associated with the MJDtr-Q78 protein, especially with its cytoplasmic aggregates.

Loss of p62 Function Causes Exacerbation of Eye Degeneration in PolyQ Disease Model Flies—To evaluate the role of p62 in the pathomechanisms of the polyQ disease model flies, we examined the effect of the loss of p62 function on eye degeneration in two different MJDtr-Q78 fly lines: MJDtr-Q78S and MJDtr-Q78W flies. The latter flies express a lower expression level of the MJDtr-Q78 protein and show milder eye degeneration than the MJDtr-Q78S flies (Fig. 2, *A*, *B*, *E*, and *I*). We used a transgenic RNAi fly line that expresses an inverted repeat RNA (IR) of *ref(2)P*, the *Drosophila* ortholog of the *p62* gene, and two different mutant fly lines of *p62*: *ref(2)P*^{od2}, bearing a deletion of the Phox and Bem1p (PB1) domain, and *ref(2)P*^{od3}, bearing a deletion of the ubiquitin-associated domain (22). We confirmed the efficient knockdown of p62 protein expression when p62-IR is expressed throughout the whole fly body by the *tub-GAL4* driver (Fig. 2, *C* and *D*). When we crossed the MJDtr-Q78S flies with the p62-IR flies or *p62* mutant flies, we found that *p62* knockdown or *p62* mutations significantly aggravate the compound eye degeneration of the MJDtr-Q78S flies, resulting in more severe depigmentation and the appearance of necrotic tissue (Fig. 2, *E–H*). Knockdown of *p62* caused more severe eye degeneration than *p62* mutations, probably because *p62* mutant flies also possess a wild-type *p62* allele in *trans* to the mutant allele. Next, we examined the effect of loss of p62 function in the MJDtr-Q78W fly line. Knockdown of *p62* or *p62* mutations caused the exacerbation of eye depigmentation (Fig. 2, *I–L*), suggesting a protective role of p62 against polyQ-induced eye degeneration. Upon quantification of the eye pigmentation by imaging analyses (Fig. 2, *Q–T*), the exacerbation of eye depigmentation by *p62* knockdown or *p62* mutations was statistically significant (Fig. 2*U*). The exacerbation by loss of